Numerical simulation of the scattering induced by a localized plume-like anomaly using a coupled spectral element and modal solution method

Y. Capdeville,[1] C. Larmat, J.–P. Vilotte,[2] and J.–P. Montagner

Département de Sismologie, Institut de Physique du Globe de Paris, France

Abstract. The possibilities of a new numerical simulation method based on the coupling of the Spectral Element Method (SEM) with a modal solution method are illustrated by experiments focusing on the scattering induced by a localized plume-like inclusion in a modified PREM. The plume is represented by a vertical cylindrical inclusion extending from the surface to the 660 km discontinuity. We present seismograms computed down to 50 s and assess the limits of a first order mode perturbation (Born approximation) method against the new numerical simulation.

Introduction

Mantle plumes are localized small scale anomalies and a challenge for seismic imaging [*Nataf*, 2000]. Their signature on the wave-field is weak and difficult to extract from the recorded data [*Ji and Nataf*, 1998; *Capdeville et al.*, 2000]. Moreover, these structures are difficult to resolve with classical perturbation theory which requires high order expansion in spherical harmonics. In this letter, the new numerical simulation method, recently developed by *Capdeville et al.* [2001] for wave propagation in global Earth models and based upon the coupling between a Spectral Element Method (SEM) and a modal solution, is shown to provide an efficient tool for this problem. The SEM has shown very promising results for realistic 3D seismic applications [*Komatitsch and Vilotte*, 1998], and has been recently extended to global Earth models [*Chaljub et al.*, 2001]. The main drawback of this method is however the computational cost which restricts the frequency that can be modeled. The new coupled method allow for higher frequency simulations by restricting the SEM to those regions inside the Earth where 3D heterogeneities are of importance while making use of a modal solution in the part of the model where a spherical symmetry can be assumed. The diffraction pattern induced by simple plume-like anomaly, defined as a vertical cylindrical inclusion within a spherically symmetric Earth model, is first computed by the coupled method. Then, the limits of a first order mode perturbation method proposed

by *Capdeville et al.* [2000] are assessed by comparison against the new numerical solution for different cylindrical radii and velocity contrasts of the plume structure. These experiments do not intend to be exhaustive but provide an illustration of this new numerical solution method both for the computation of synthetic seismograms in 3D Earth models and for assessing the limits of the approximations generally used in global seismology.

The Method

The numerical method [*Capdeville et al.*, 2001] is based on the partition of the earth into an outer shell, in which 3D heterogeneities are confined, and an inner spherically symmetric sphere (see Figure 1). The domains are connected through a spherical interface. Depending on the problem, the outer shell can be the whole mantle, a portion of the upper mantle or the crust. In the outer shell, the solution is sought in terms of the SEM, based on a high order variational formulation in space and a second order explicit time scheme [*Komatitsch and Vilotte*, 1998]. Using a central projection transformation [*Chaljub et al.*, 2001], the outer shell is discretized almost uniformly by hexahedra elements avoiding the pole problems of the spherical coordinates. High resolution can be achieved, for realistic Earth models, using non-conforming mesh refinements [*Chaljub et al.*, 2001]. In the inner sphere, the solution is based upon a modal method in frequency after a spherical harmonic expansion. Using the continuity conditions of both traction and displacement, the modal solution allows to build explicitly the interface operator that characterizes the coupling between the two methods and provides, for the outer shell, the traction along the interface as a response of the inner sphere to a surface displacement distribution [*Capdeville et al.*, 2001]. In the SEM, it is introduced as a dynamic boundary condition and significantly reduces the computational cost. However, the construction of the interface operator is only explicit in the frequency and spherical harmonics domains. The back transformation in the space and time domain is not strait-forward and requires to derive an asymptotic solution for the high frequencies of the modal solution [*Capdeville et al.*, 2001].

Figure 1

The plume here is a simple vertical cylindrical anomaly, in a spherically symmetric Earth model, with the temperature structure proposed by *Farnetani* [1997]. The perturbation in temperature is linearly related to velocity and density anomalies according to *Kumazawa and Anderson* [1969]. The spherically symmetric Earth model, PREM–light, is a modified PREM [*Dziewonski and Anderson*, 1981], where the uppermost

crustal thin layers are smoothed out. The plume-like anomaly extends from the surface down to the 660 km discontinuity defined as the coupling interface. The Figure 2 shows the SEM mesh and the S-wave velocity contrast.

Figure 2

Direct numerical simulation

In this experiment, the source is an explosion at 163 km depth with a frequency cutoff of 20 mHz. The epicentral distance between the source and the plume axis is 30°. The maximum contrast, in the plume, for the P and S-wave velocities are 4.5% and 3.6% respectively and for the density 1.8%. Two radii of 100 km and 250 km have been used for the plume. These parameters are reasonable compared to what is expected [*Wolfe et al.*, 1997; *Allen et al.*, 1999]. The ratio between the dominant propagating wavelength and the plume radius is of the order of one for both radii : greater than one in the former and smaller than one in the latter.

Let us first examine the radiation patterns of these plumes. To do so, receivers are set on a 30° angular radius circle around the plume and are locate by the scattering angle φ (see Figure 3, top). We call radiation pattern, the scattered wavefield in time, defined as the difference between the signals computed with and without the plume inclusion, as a function of the scattering angle. The vertical component of the radiation pattern is shown Figure 3, for the two plume radii. Even though the radiation pattern depends upon the lateral extent of the plume, the maximum scattered amplitude, for both plumes, is in the forward direction, with a small backward scattering and almost no lateral scattering. The forward maximum, which, for its late part, is mainly due to the perturbation that corrects for the surface wave phase, increases with the plume radius, as expected [*Capdeville et al.*, 2000]. The radiation pattern is complex, due to the wide source spectrum (a Ricker wavelet), and is dominated by the Rayleigh-to-Rayleigh radiation pattern.

Figure 3

The vertical component of the scattered signal produced by the small plume, recorded along the source-plume line, is shown on Figure 4. The phases are difficult to individualize due to the low frequency and the wide spectrum of the source. After the first P-phases, the signal is dominated by the scattered Rayleigh phase. An amplified phase emerges from the scattered S- and X-phases. The latter corresponds, in terms of body waves, to a superposition of P-wave subsurface reflections. The amplified phase is probably due to a focusing of the waves propagating almost vertically in the crust and the upper mantle. Even though the depth sensitiv-

Figure 4

ity of surface waves increases as the frequency decreases, at low frequency the amplitude of the scattered signal is very weak (2% of the incoming wave) and will be difficult to extract from the actual data.

Comparison with first order normal mode perturbation

The synthetic seismograms computed using a first order normal mode perturbation method [*Capdeville et al.*, 2000], are compared against those obtained by the new method. The perturbation method for a localized anomaly requires to couple a large number of modes. To reduce the computation time of the perturbation method, the bandwidth of the source spectrum is restricted to a cutoff period of 100 s. The source is an explosion at 161 km depth and at an angular distance of 60° from the plume. Two plumes are considered. Plume A has a radius of 200 km with a maximum contrast for P and S-wave velocities of respectively 4.5% and 3.6% and for the density of 1.8%. For this low velocity contrast, the perturbation method is expected to be accurate. Plume B has a radius of 400 km with a maximum contrast for P and S-wave velocities of respectively 19% and 15.5% and for the density of 7.6%. In contrast, the perturbation method for these extreme values is expected to reach its limits. Three receiver positions are considered (see sketch, top of Figure 5) : one on the top of the plume (receiver 0) and two at a constant angular distance from the plume, but a different scattering angle (receivers 1 and 2)

Figure 5

First, a comparison between the synthetic vertical components at receiver 0, is shown on Figure 5 for both plumes. In the perturbation method, for such a receiver location and localize heterogeneity, spurious trains, inherent to the numerical cutoff in the mode coupling, arrive at the same time as scattered signals and need to be minimized with an optimal high $\Delta\ell$, depending on the shape of the anomaly and on the incident wavelength [*Capdeville et al.*, 2000]. Here, harmonics from $n = 0$ to 8 are used with a full coupling of modes up to $\Delta\ell = \pm 40$. For plume A, the agreement is very good. The fact that only the nine five harmonics have been used in the perturbation method explains the discrepancy of the early arrivals. The expected inaccuracy of the perturbation method for this receiver does not allow further interpretation of small differences on amplitude. For plume B, the scattered Rayleigh wave is, surprisingly, accurately modeled by the perturbation method.

For receivers 1 and 2, harmonics from $n = 0$ to 4 have been used with $\Delta\ell = \pm 20$ (spurious train effects are not critical here). For plume A, both methods are,

as expected, in good agreement. The slight difference in amplitude can be related to the perturbation method : inaccuracy of the integration over the localized heterogeneity and numerical coupling cutoff. For plume B, the perturbation method does not compare well with the numerical solution method. At receiver 1, if the comparison in amplitude is reasonably good, but the predicted phases are now quite different. The situation is even worse at receiver 2 for both amplitude and phase. In this case, second and higher order effects become important.

A comparison between the transverse components is finally shown on Figure 5 for receiver 2, the only receiver where this component is not zero. In the case of wave conversion, the coupling along a same branch is no more dominant and, to improve the accuracy, a coupling of $n = 0$ to 8 is performed up to $\Delta\ell = \pm 40$. For plume A, the phase agreement is very good, despite a small error in amplitude of the same origin as previously. For plume B, neither the amplitude nor the phase computed by the perturbation method agree with the direct solution method.

Within this limited number of experiments, the perturbation approach is more accurate and stable than expected. Nevertheless it faces severe limitations avoided using the direct numerical simulation method. In particular, the accuracy is controlled by the coupling cutoff $\Delta\ell$, which depends on the shape of the anomaly, the incident wavelength, and the receiver location. This leads to limitations in terms of frequency not considering those associated with body waves.

Conclusion

Potentialities of a new numerical simulation method, based on the coupling of the SEM with a modal solution method, have been presented. The method allows to compute the whole wavefield for localized plume-like anomalies at frequencies and for velocity contrasts that would not be possible using a perturbation method. It can also assess the validity of classical approximations used to compute synthetic seismograms in global tomography. The examples have been computed on a relatively small cluster architecture : 16 processors and less than 4 GB distributed memory. Medium size architectures allow for simulations down to a period of 20 s or less. The method can be applied to a large number of global seismology problems. The coupling method is now extended to a spectral element strip between an inner sphere and an outer shell where the solution is sought with a modal solution method. This should allow to investigate the D" layer down to probably less

than 10 s.

Acknowledgments. Thanks to Emmanuel Chaljub and S. Singh for helpful discussions. The computations were made possible by the DMPN with the support of the CNRS, the MRT and the Région Ile de France.

References

Allen, R., G. Nolet, W. Morgan, K. Vogfjörd, and B. B. et al., The thin hot plume beneath Iceland, *Geophys. J. Int.*, *137*, 51–63, 1999.

Capdeville, Y., E. Stutzmann, and J. P. Montagner, Effect of a plume on long period surface waves computed with normal modes coupling, *Phys. Earth Planet. Inter.*, *119*, 57–74, 2000.

Capdeville, Y., E. Chaljub, J. P. Vilotte, and J. P. Montagner, Computation of the complete elastic wavefield in global eath models by using a coupled method of spectral elements and modal solution, *Geophys. J. Int.*, p. submitted, 2001.

Chaljub, E., J.-P. Vilotte, and Y. Capdeville, Solving elastodynamics in a solid heterogeneous 3-Sphere: a parallel spectral element approximation on non-conforming grids, *Int. J. Num. Meth.*, submitted, 2001.

Dziewonski, A. M., and D. L. Anderson, Preliminary reference Earth model, *Phys. Earth Planet. Inter.*, *25*, 297–356, 1981.

Farnetani, C. G., Excess temperature of mantle plumes: The role of chemical stratification across D", *Geophys. Res. Lett.*, *24*, 1583–1586, 1997.

Komatitsch, D., and J. P. Vilotte, The spectral element method: an effective tool to simulate the seismic response of 2D and 3D geological structures, *Bull. Seism. Soc. Am.*, *88*, 368–392, 1998.

Kumazawa, M., and O. L. Anderson, Elastic Moduli, Pressure Derivatives, and Temperature Derivatives of Singe–Crystal Olivine and Single–Crystal Forsterite, *J. Geophys. Res.*, *74*, 5961–5972, 1969.

Nataf, H.-C., Seismic imaging of mantle plumes, *Annu. Rev. Earth Planet. Sci.*, *28*, 391–417, 2000.

Wolfe, C. J., I. T. Bjarnason, J. C. VanDecar, and S. C. Solomon, Seismic structure of the Iceland mantle plume, *Nature*, *385*, 245–247, 1997.

Ji, Y., and H. C. Nataf, Detection of mantle plumes in the lower mantle by diffraction tomography: theory, *Earth Planet. Sci. Lett.*, *159*, 87–98, 1998.

Y. Capdeville, Seismological Laboratory of Berkeley, 215 McCone Hall, Berkeley, CA 94720–4760, USA. (e-mail: yann@seismo.berkeley.edu)

C. Larmat, J.P. Vilotte and J.P. Montagner, Département de Simologie, Institut de Physique du Globe de Paris, 4 place Jussieu, Case 89, 75252 Paris cedex 05, France. (e-mail: larmat@ipgp.jussieu.fr; vilotte@ipgp.jussieu.fr; jpm@ipgp.jussieu.fr;)

(Received _____)

---

[1]Now at Seismological laboratory, UC Berkeley, California

[2]Also at Département de Modélisation Physique et Numérique, Institut de Physique du Globe de Paris, France

Figure 1. The Earth model is partitioned in two parts: the SEM is used in the outer shell, the Modal Solution (MS) is used in the inner sphere and is coupled with the SEM on a spherical coupling interface.

Figure 1. The Earth model is partitioned in two parts: the SEM is used in the outer shell, the Modal Solution (MS) is used in the inner sphere and is coupled with the SEM on a spherical coupling interface.

Figure 2. Left: global view of the model where two regions have been removed for sake of visibility. The SEM mesh is drawn only for two regions. Right: zoom on the plume inclusion area.The colors indicate the S wave velocity contrast with respect to the PREM –light reference model. On this figure, the plume radius is of 250 km and the maximum S-velocity contrast is 4.5%.

Figure 2. Left: global view of the model where two regions have been removed for sake of visibility. The SEM mesh is drawn only for two regions. Right: zoom on the plume inclusion area.The colors indicate the S wave velocity contrast with respect to the PREM –light reference model. On this figure, the plume radius is of 250 km and the maximum S-velocity contrast is 4.5%.

Figure 3. Vertical component of the scattered field, as a function of the scattering angle φ (see sketch on top), for two plume-like cylindrical structures of 100 km radius (left) and 250 km radius (right). The forward scattering pattern increases with the plume radius. The maximum scattering amplitude is related to surface waves.

Figure 3. Vertical component of the scattered field, as a function of the scattering angle φ (see sketch on top), for two plume-like cylindrical structures of 100 km radius (left) and 250 km radius (right). The forward scattering pattern increases with the plume radius. The maximum scattering amplitude is related to surface waves.

Figure 4. Vertical component of the scattered field for the small plume (plume 1), at four angular distances along the source-plume great circle : -1, 0, 1 and 2 degrees from the plume. The arrow indicates a scattered amplified phase for the receiver on top of the plume.

Figure 4. Vertical component of the scattered field for the small plume (plume 1), at four angular distances along the source-plume great circle : -1, 0, 1 and 2 degrees from the plume. The arrow indicates a scattered amplified phase for the receiver on top of the plume.

Figure 5. Scattered field obtain by the coupled method (solid line) and the perturbation method (dotted line), for plume A (left) and plume B (right), at receivers 0, 1 and 2. The receiver positions are shown on top sketch.

Figure 5. Scattered field obtain by the coupled method (solid line) and the perturbation method (dotted line), for plume A (left) and plume B (right), at receivers 0, 1 and 2. The receiver positions are shown on top sketch.

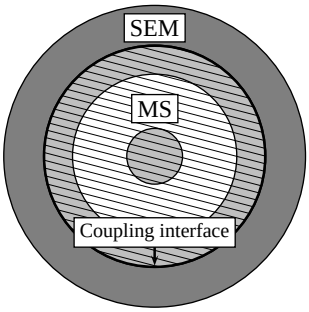

Figure 1

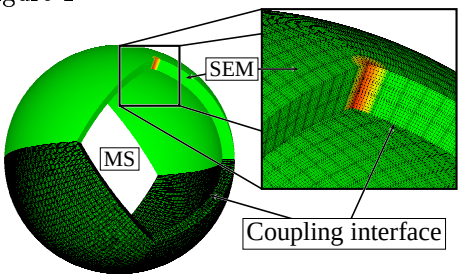

Figure 2

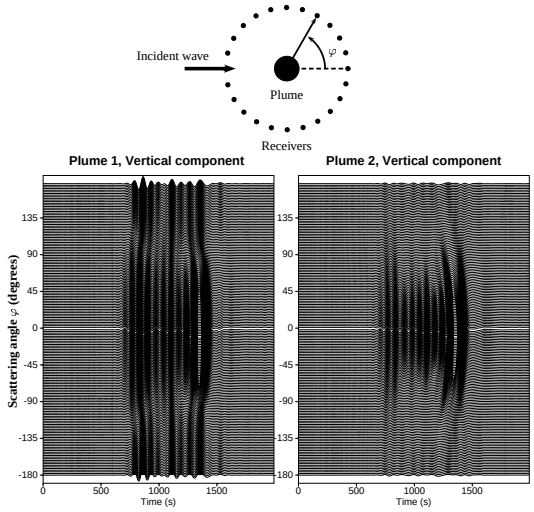

Figure 3

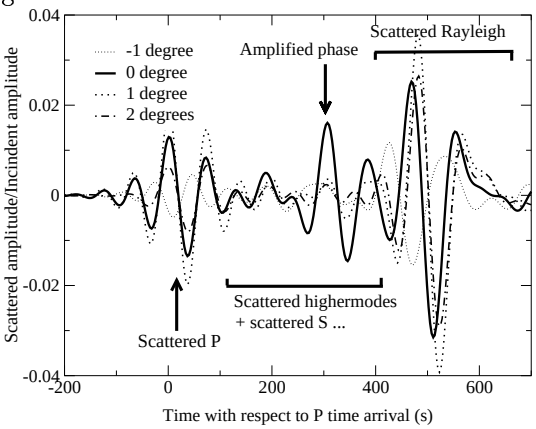

Figure 4

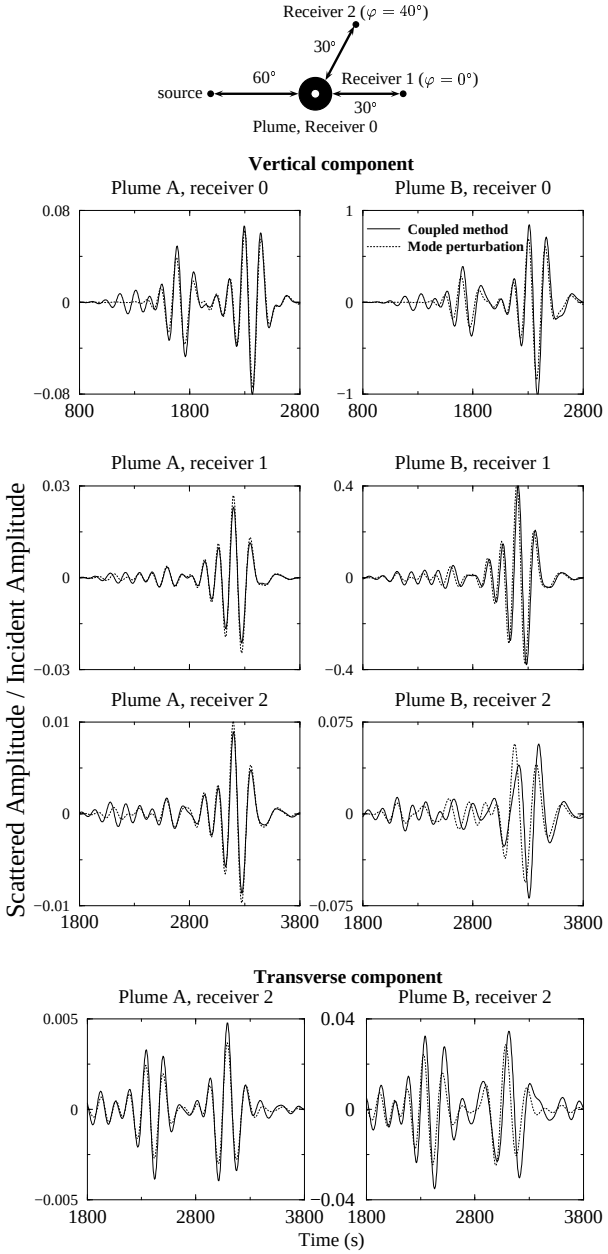

Figure 5

CAPDEVILLE ET AL.: NUMERICAL SIMULATION OF PLUME SCATTERING

CAPDEVILLE ET AL.: NUMERICAL SIMULATION OF PLUME SCATTERING

CAPDEVILLE ET AL.: NUMERICAL SIMULATION OF PLUME SCATTERING

CAPDEVILLE ET AL.: NUMERICAL SIMULATION OF PLUME SCATTERING

CAPDEVILLE ET AL.: NUMERICAL SIMULATION OF PLUME SCATTERING

CAPDEVILLE ET AL.: NUMERICAL SIMULATION OF PLUME SCATTERING

CAPDEVILLE ET AL.: NUMERICAL SIMULATION OF PLUME SCATTERING

CAPDEVILLE ET AL.: NUMERICAL SIMULATION OF PLUME SCATTERING

CAPDEVILLE ET AL.: NUMERICAL SIMULATION OF PLUME SCATTERING

CAPDEVILLE ET AL.: NUMERICAL SIMULATION OF PLUME SCATTERING

CAPDEVILLE ET AL.: NUMERICAL SIMULATION OF PLUME SCATTERING

CAPDEVILLE ET AL.: NUMERICAL SIMULATION OF PLUME SCATTERING

CAPDEVILLE ET AL.: NUMERICAL SIMULATION OF PLUME SCATTERING

CAPDEVILLE ET AL.: NUMERICAL SIMULATION OF PLUME SCATTERING

CAPDEVILLE ET AL.: NUMERICAL SIMULATION OF PLUME SCATTERING

CAPDEVILLE ET AL.: NUMERICAL SIMULATION OF PLUME SCATTERING

CAPDEVILLE ET AL.: NUMERICAL SIMULATION OF PLUME SCATTERING

CAPDEVILLE ET AL.: NUMERICAL SIMULATION OF PLUME SCATTERING